Particle generation through energy discretization and restrictive planes in GEANT4 simulations for potential applications of cosmic ray muon tomography

A. Ilker Topuz[1,2], Madis Kiisk[1,3], Andrea Giammanco[2]

[1] Institute of Physics, University of Tartu, W. Ostwaldi 1, 50411, Tartu, Estonia
[2] Centre for Cosmology, Particle Physics and Phenomenology, Université catholique de Louvain, Chemin du Cyclotron 2, B-1348 Louvain-la-Neuve, Belgium
[3] GScan OU, Maealuse 2/1, 12618 Tallinn, Estonia

E-mail: ahmet.ilker.topuz@ut.ee, ahmet.topuz@uclouvain.be

Abstract. In this study, by attempting to resolve the difficulties related to the angular distribution during the particle generation for the muon tomography applications in the GEANT4 simulations, we exhibit an unconventional methodology that is hinged on the direction limitation via the vectorial construction from the generation location to the restriction area rather than using a certain angular distribution or interval. In other words, we favor a momentum direction that is determined by a vector constructed between an initial point randomly chosen on a generative point/plane and a second point arbitrarily selected on a restrictive plane of the same dimensions with the basal cross section of the volume-of-interest (VOI). On account of setting out such a generation scheme, we optimize the particle loss by keeping an angular acceptance that is directly dependent on the VOI geometry as well as the vertical position of the restrictive plane for a tomographic system of a finite size. We demonstrate our strategy for a set of target materials including aluminum, iron, copper, lead, and uranium with a dimension of $40\times10\times40$ cm^3 over three restrictive planes of different positions by using a discrete energy spectrum between 0.1 and 8 GeV and we compute the scattering angle, the number of absorption, and the particle loss. Upon our simulation outcomes, we show that the particle generation by means of restrictive planes is an effective strategy that is flexible towards a variety of computational objectives in the GEANT4 simulations.

Keywords: Muon tomography; Characteristic parameters; Energy discretization; Restrictive planes; Source biasing; Non-analogue Monte Carlo simulations; GEANT4

1. Introduction

The emerging applications of cosmic ray muon tomography [1, 2, 3] lead to a significant rise in the utilization of the cosmic particle generators, e.g. CRY [4], CORSIKA [5], or CMSCGEN [6], where the fundamental parameters such as the energy spectrum and the angular distribution associated with the generated muons are represented in the continuous forms routinely governed by the probability density functions over the corresponding vast intervals. Despite this perceptible increase in the diversity of the muon generators, the common difficulties in the hands-on applications that might be relatively exemplified as perplexing coupling with the Monte Carlo

codes, unnecessarily broad and occasionally unmodifiable parametric intervals for the specific applications, extensive execution times, and complications in the particle tracking partly remain steady. Contrary to the continuous mode, the discretized energy spectra, i.e. multi-group energy approximations to put it another way, have been ubiquitously employed in the neighboring fields such as nuclear engineering [7, 8] and medical physics [9, 10] under the umbrella of the non-analogue Monte Carlo simulations [11] on and on. Along with the discretization schemes based on the theoretical assumptions, a number of notable empirical studies founded on the advanced particle detectors such as the BESS spectrometer [12] represent the experimental energy spectra in the discrete format. While MNCP6 [13] includes the necessary algorithms to utilize the discrete energy distributions in the black box paradigm, the general particle source (GPS) in GEANT4 [14] is the existing pre-configured module that provides the opportunity of this discrete approach through a macro file without detailing the algebraic/algorithmic phase.

The wide angular distribution [15] of the incoming cosmic ray muons in connection with either incident angle or azimuthal angle is a challenging trait that leads to a drastic particle loss in the course of parametric computations through the GEANT4 [14] simulations associated with the muon tomography [1, 2, 3] since the tomographic configurations as well as the target geometries also influence the number of the detected particles apart from the generation strategies. To further detail, the basic parameters such as the scattering angle, the particle displacement, and the particle absorption owing to the volume-of-interest (VOI) *de facto* dictate the particle penetration through the multiple sections of the tomographic setup in addition to the VOI. Hence, a number of the loss cases notably come into effect unless the calculation conditions are fulfilled, and not only the computation statistics and the numerical outcomes but also the initial assumptions like the energy spectrum are also perturbed since the VOI accepts a significantly lower number of particles in the instance of the substantial particle loss. While a number of source biasing techniques [11] are offered by MCNP6 [16, 13] in the black box format under the class of non-analogue Monte Carlo simulations, the GEANT4 simulations are usually constrained to the existing particle generators or the general particle source (GPS) unless G4ParticleGun is preferred. Motivated by the excessive particle loss and its effect on the computation time as well as the characteristic parameters identified in the muon tomography, we set forth in the present study a scheme that is hinged on the particle generation through the planar restriction by means of the vectorial construction over our tomographic setup consisting of plastic scintillators manufactured from polyvinyl toluene with the dimensions of $100\times0.4\times100$ cm^3. This study is organized as follows. In section 2, we exhibit the discrete probabilities for the corresponding discrete energies and we describe the implementation in the GEANT4 code. In section 3, we elucidate our methodology based on the restrictive planes and we express our characteristic parameters as well as our simulation features in section 4. While we disclose our simulation outcomes in section 5, we draw our conclusions in section 6.

2. Energy discretization and its implementation in GEANT4

At the outset, we aim at discretizing the energy spectrum based on the extracted energy list from the CRY muon generator [4] between 0 and 8 GeV. To achieve this aim, we first set out our constant bin length that is selected as 0.1 GeV. Then, in agreement with the energy dataset acquired through the CRY generator, the number of the counts in the specific energy bin denoted by E_i in GeV is computed by incorporating any $E_x \in (E_{i-1}, E_i]$ under the condition of $m_0 = 0$ for $E_0 = 0$. While this operation is an approximation by definition, we do not significantly neglect any fundamental information in the case of the fine energy bins as accomplished in the present study, which also implies that the simulation outcomes by means of the finely binned histogram do not yield consequential differences in comparison with the continuous energy spectra. Whereas the count numbers in the particular energy bins already provide an opportunity to employ the discrete energy distributions in the wake of renormalization, we

favor to determine the discrete probabilities that serve to constitute a probability grid; hence, we first calculate the total count over 80 energy bins. In the end, the discrete probability, i.e. the discrete normalized frequency to rephrase it, at a given energy bin indicated by E_i is the ratio between the specific count in E_i and the total counts over 80 bins by satisfying the unity condition. Finally, we tabulate the discrete probabilities along with the discrete muon energies obtained via the CRY muon source in Table 1 by entitling D¬CRY. As indicated in Table 1, we view that the highest discrete probability appertains to the energy bin of 0.5 GeV, i.e. the mode of our discrete energy distribution, which is reduced approximately by one order of magnitude at 8 GeV, and the trend observed in D¬CRY resembles to a log-normal distribution with a positive skewness.

Table 1. D¬CRY discrete probabilities between 0 and 8 GeV.

E_i [GeV]	p_i	E_i [GeV]	p_i	E_i [GeV]	p_i
0.0	0.0000	2.7	0.0147	5.4	0.0061
0.1	0.0125	2.8	0.0142	5.5	0.0063
0.2	0.0257	2.9	0.0141	5.6	0.0066
0.3	0.0280	3.0	0.0128	5.7	0.0065
0.4	0.0270	3.1	0.0126	5.8	0.0056
0.5	0.0352	3.2	0.0121	5.9	0.0058
0.6	0.0282	3.3	0.0129	6.0	0.0058
0.7	0.0315	3.4	0.0124	6.1	0.0057
0.8	0.0307	3.5	0.0119	6.2	0.0055
0.9	0.0277	3.6	0.0106	6.3	0.0055
1.0	0.0254	3.7	0.0105	6.4	0.0043
1.1	0.0315	3.8	0.0096	6.5	0.0043
1.2	0.0281	3.9	0.0103	6.6	0.0040
1.3	0.0258	4.0	0.0092	6.7	0.0036
1.4	0.0236	4.1	0.0087	6.8	0.0039
1.5	0.0217	4.2	0.0088	6.9	0.0038
1.6	0.0215	4.3	0.0079	7.0	0.0039
1.7	0.0234	4.4	0.0078	7.1	0.0043
1.8	0.0213	4.5	0.0076	7.2	0.0036
1.9	0.0196	4.6	0.0070	7.3	0.0036
2.0	0.0203	4.7	0.0073	7.4	0.0036
2.1	0.0184	4.8	0.0071	7.5	0.0041
2.2	0.0171	4.9	0.0072	7.6	0.0033
2.3	0.0170	5.0	0.0069	7.7	0.0035
2.4	0.0162	5.1	0.0064	7.8	0.0036
2.5	0.0153	5.2	0.0067	7.9	0.0034
2.6	0.0153	5.3	0.0067	8.0	0.0035

In order to qualitatively show the variation of D¬CRY, Fig. 1 displays the energy histogram of D¬CRY in comparison with the discrete CMSCGEN data reproduced from another study [17] that is dedicated to the CMS strip tracker.

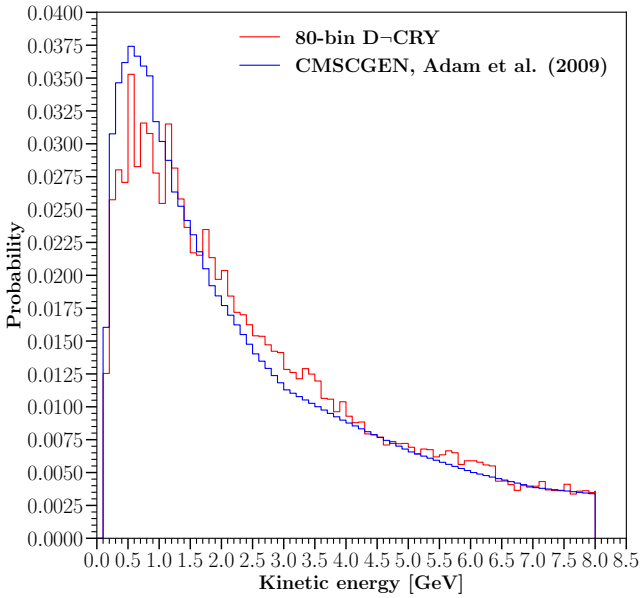

Figure 1. Energy histograms of 80-bin D¬CRY compared to CMSCGEN.

After the discrete energy spectrum, we subsequently integrate our strategy to inject the incoming muons by means of G4ParticleGun. By reminding the unity condition, we build a grid by adding up the discrete probabilities, the interval of which starts with 0 and ends in 1 as illustrated in Fig. 2. Thus, each cell in this grid, i.e. the difference between two points on the probability grid, specifies a discrete probability. Then, we generate a random number denoted by ξ between 0 and 1 by using the pre-defined uniform number generator called G4UniformRand(). Finally, we scan this random number on the probability grid by checking the difference between the grid points and we assign the particular discrete energy when the random number matches with the associated cell.

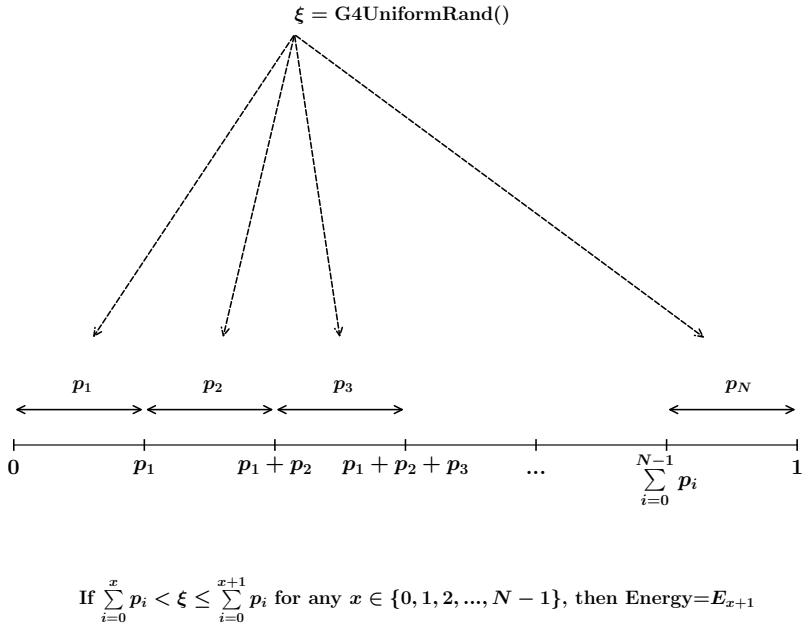

Figure 2. Scheme of probability grid implemented via G4ParticleGun in GEANT4.

3. Generation via planar restriction

To begin with, we principally exhibit two planar restrictive schemes to be adapted in GEANT4 as illustrated in Fig. 3 where (a) shows the particle generation from a fixed point as well as the direction restriction by means of a restrictive pseudo-plane, whereas (b) demonstrates the randomly picked up particles from a generative plane, the directions of which are projected into a similar restrictive plane.

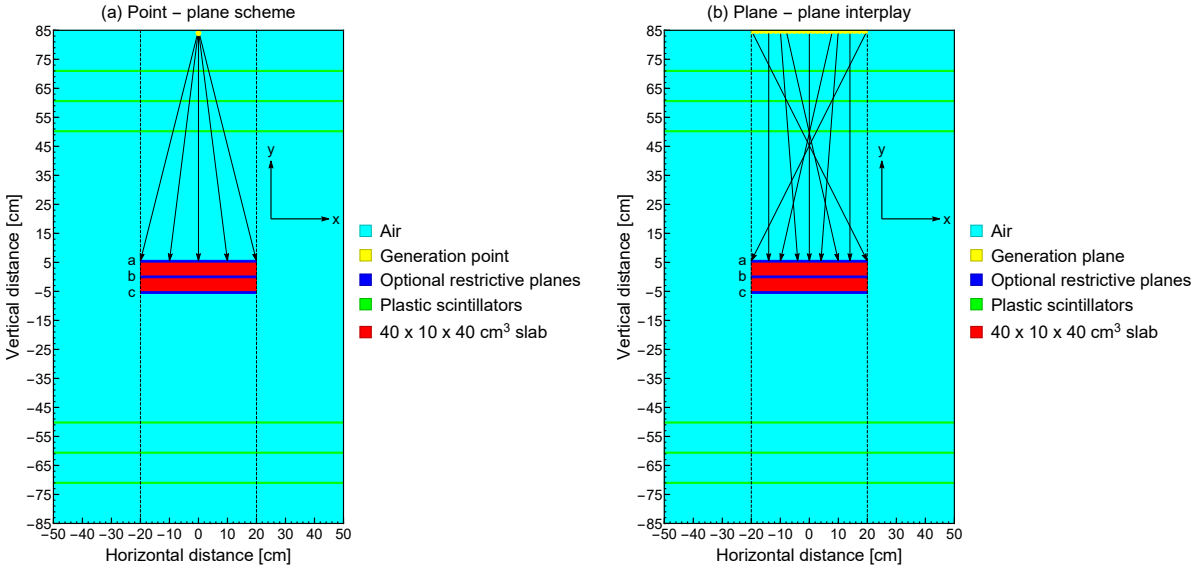

Figure 3. Depiction of particle generation through restrictive planes in GEANT4 (a) generative point - restrictive plane scheme and (b) generative - restrictive planar interplay.

In order to practically outline the present methodology that is initially described in Fig. 3(a), the particle location in cm on the central point at height=85 cm is listed as written in

$$x_0 = 0, \quad y_0 = 85, \quad z_0 = 0 \tag{1}$$

Subsequently, the limited location in cm on any restrictive plane of $2L \times 2D$ cm^2 is noted as shown in

$$x_1 = -L + 2 \times L \times \text{G4UniformRand}(), \quad y_1 = \text{constant}, \quad z_1 = -D + 2 \times D \times \text{G4UniformRand}() \tag{2}$$

Here, G4UniformRand() is the uniform random number generator between 0 and 1, which is predefined in GEANT4. Then, by constructing a vector from the generative point to the restrictive plane, we obtain

$$px = x_1 - x_0 = x_1, \quad py = y_1 - y_0, \quad pz = z_1 - z_0 = z_1 \tag{3}$$

Thus, the selective momentum direction, i.e. $\vec{P} = (P_x, P_y, P_z)$, is

$$P_x = \frac{px}{\sqrt{px^2 + py^2 + pz^2}}, \quad P_y = \frac{py}{\sqrt{px^2 + py^2 + pz^2}}, \quad P_z = \frac{pz}{\sqrt{px^2 + py^2 + pz^2}} \tag{4}$$

The latter scheme that assumes a planar generation as delineated in Fig. 3(b) entails particle locations in cm on the generative plane of $2L \times 2D$ cm^2 as written in

$$x_0 = -L + 2 \times L \times \text{G4UniformRand}(), \quad y_0 = 85, \quad z_0 = -D + 2 \times D \times \text{G4UniformRand}() \tag{5}$$

As performed in Eq. (2) for the previous scheme, the limited locations in cm on any restrictive plane of $2L \times 2D$ cm^2 are selected from

$$x_1 = -L{+}2{\times}L{\times}\text{G4UniformRand}(), \quad y_1 = \text{constant}, \quad z_1 = -D{+}2{\times}D{\times}\text{G4UniformRand}() \quad (6)$$

Additionally, via a vector construction between two planes, we acquire anew

$$px = x_1 - x_0, \quad py = y_1 - y_0, \quad pz = z_1 - z_0 \quad (7)$$

Therefore, the selective momentum direction denoted by $\vec{P} = (P_x, P_y, P_z)$ is again

$$P_x = \frac{px}{\sqrt{px^2 + py^2 + pz^2}}, \quad P_y = \frac{py}{\sqrt{px^2 + py^2 + pz^2}}, \quad P_z = \frac{pz}{\sqrt{px^2 + py^2 + pz^2}} \quad (8)$$

The initial particle positions and the selective momentum directions are incorporated by using G4ParticleGun. The simulation previews through both the restrictive schemes are displayed in Fig. 4 where (a) indicates the particles generated from a fixed point, while (b) presents the randomly generated particles from a fixed plane.

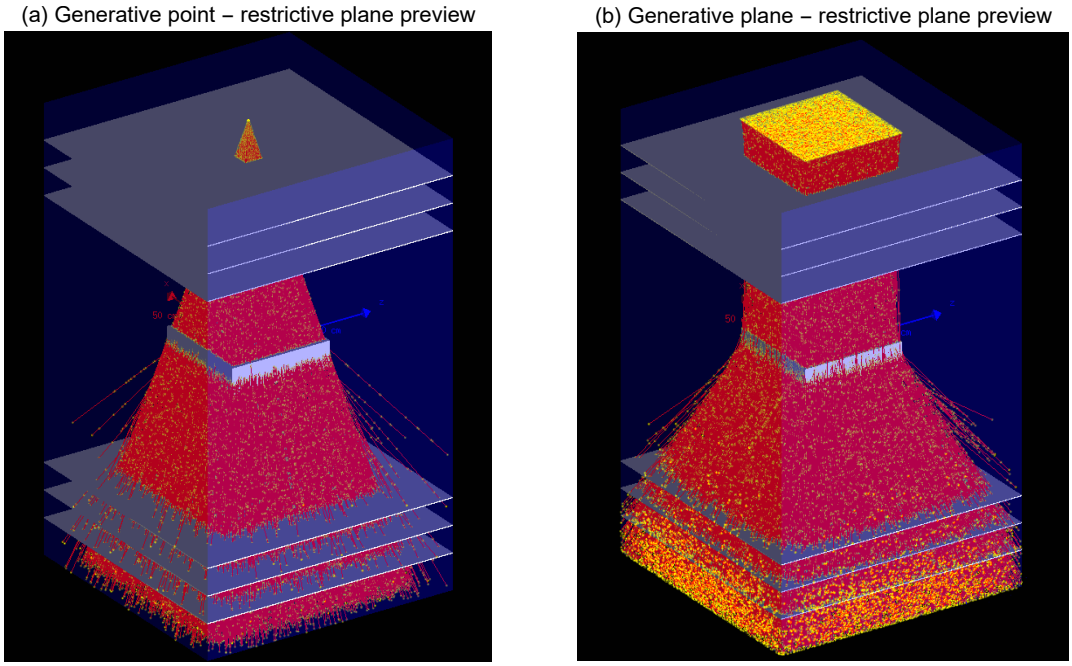

Figure 4. Simulation previews by using restrictive plane b for copper in GEANT4 (a) point - plane scheme and (b) plane - plane scheme.

It is worth mentioning that neither generation points/planes nor restrictive planes are subject to any limitation in terms of shape, size, or location since our recent concept is preferred in the first instance for the sake of simplicity. On top of this, it is also possible to prefer different distributions especially already implemented in GEANT4, e.g. Gauss or Poisson distribution depending on the envisaged application.

4. Characteristic parameters and simulation setup

Befor testing our schemes, we express our characteristic parameters to be computed at the end of the GEANT4 simulations. The average scattering angle due to the target volume and its

standard deviation over N number of the non-absorbed/non-decayed muons is determined as expressed in [18, 19, 20]

$$\bar{\theta} \pm \delta\theta = \frac{1}{N}\sum_{i=1}^{N}\theta_i \pm \sqrt{\frac{1}{N}\sum_{j=1}^{N}(\theta_j - \bar{\theta})^2} \tag{9}$$

Additionally, the root-mean-square (RMS) of the scattering angle over N number of the non-absorbed/non-decayed muons is calculated by using the following expression:

$$\theta_{\mathrm{RMS}} = \sqrt{\frac{1}{N}\sum_{i=1}^{N}\theta_i^2} \tag{10}$$

Along with the scattering angle, we track the number of the absorbed muons within the VOI as denoted in

$$\#_{\mathrm{Capture}}^{\mathrm{In-target}} = \#\text{ of muMinusCaptureAtRest in VOI} \tag{11}$$

Last but not least, we define the particle loss entitled off-target loss as follows

$$\#_{\mathrm{Loss}}^{\mathrm{Off-target}} \approx \underbrace{\#_{\mathrm{Out-scattering}}}_{\text{Characteristic}} + \underbrace{\#_{\mathrm{Decay}}}_{\text{Negligible}} + \underbrace{\#_{\mathrm{Capture}}^{\mathrm{Off-target}}}_{\text{Negligible}} + \underbrace{\#_{\mathrm{Deflection}}^{\mathrm{Initial}}}_{\text{Occasional}} \tag{12}$$

where $\#_{\mathrm{Out-scattering}}$ is the number of the scattered muons from the VOI by leaking out of the tomographic device, $\#_{\mathrm{Decay}}$ is the negligible number of the decayed muons into electrons/positrons, $\#_{\mathrm{Capture}}^{\mathrm{Off-target}}$ is the insignificant number of the absorbed muons outside the VOI, and $\#_{\mathrm{Deflection}}^{\mathrm{Initial}}$ is the number of muons that miss the VOI only in the case of the wide beams, which occasionally occurs due to the barriers before the VOI despite the initial restricted orientation to the VOI boundary, i.e. the tiny deflection owing to the detector layers.

Table 2. Simulation features.

Particle	μ^-
Momentum direction	Restrictive downward
Beam geometry	Prismatic
Initial position (cm)	y=85
Particle injector	G4ParticleGun
Number of particles	10^5
Energy distribution	Non-linear discrete
Energy interval	[0, 8]
Enegy bin step length (GeV)	0.1
Target geometry	Rectangular prism
Target volume (cm^3)	40×10×40
Material database	G4/NIST
Reference physics list	FTFP_BERT

Our simulation features are summarized in Table 2, and we use a 80-bin discrete muon energy spectrum extracted from the CRY generator [4] between 0 and 8 GeV. The muon tracking is accomplished by G4Step, and the recorded hit positions on the detector layers are post-processed by means of a Python script.

5. Simulation outcomes

We asses our methodology over our tomographic configuration described in Fig. 3(a)-(b) and we select our set of materials and the VOI geometry in accordance with another study [21] dedicated to the muon tomography where the material list consists of aluminum, iron, copper, lead, and

uranium, and the target geometry is composed of a rectangular prism with the dimensions of $40\times10\times40$ cm^3. As indicated in Fig. 3, we contrast three restrictive planes labeled as a, b, and c that are placed atop the VOI, amidst the VOI, and beneath the VOI, respectively. We commence with the first scheme that is based on the point - plane generation, and the simulation outcomes by using restrictive plane a are listed in Table 3.

Table 3. Point - plane scheme, restrictive plane a, thickness=10 cm.

Material	$\bar{\theta} \pm \delta\theta$ [mrad]	θ_{RMS} [mrad]	$\#^{\mathrm{In-target}}_{\mathrm{Capture}} \pm \delta$Capture	$\#^{\mathrm{Off-target}}_{\mathrm{Loss}} \pm \delta$Loss
Aluminum	14.9±25.7	29.7	-	516±23
Iron	33.0±47.4	57.8	1073±33	541±23
Copper	37.4±55.5	66.9	1083±33	616±25
Lead	59.5±81.9	101.2	1135±34	1215±35
Uranium	73.7±91.1	117.2	3267±57	1542±39

As shown in Table 3, the computed parameters including the particle loss show a characteristic tendency depending on the atomic number as well as the material density for a fixed thickness. Although the muon beam is already directed to the VOI boundary even in the case of restrictive plane a, which leads to an immoderate reduction in the particle loss compared to the conventional approaches, a remarkable number of the loss events in agreement with the intrinsic properties of the target material are still observed.

Table 4. Point - plane scheme, restrictive plane b, thickness=10 cm.

Material	$\bar{\theta} \pm \delta\theta$ [mrad]	θ_{RMS} [mrad]	$\#^{\mathrm{In-target}}_{\mathrm{Capture}} \pm \delta$Capture	$\#^{\mathrm{Off-target}}_{\mathrm{Loss}} \pm \delta$Loss
Aluminum	15.7±26.4	30.7	-	54±7
Iron	35.3±50.1	61.3	1172±34	133±12
Copper	39.5±57.0	69.3	1179±34	216±15
Lead	63.2±84.2	105.2	1220±35	833±29
Uranium	78.2±93.6	121.4	3604±60	1187±34

In order to see the positional effect of the planar restriction, the simulation outcomes from restrictive plane b are tabulated in Table 4. In comparison with Table 3, we observe that the characteristic parameters except the particle loss slightly change when the muon beam is narrowed by using restrictive plane b; however, the particle loss manifests a minimum reduction of 31% as opposed to restrictive plane a. Whereas restrictive plane b is capable of diminishing the particle loss by a factor of order in certain cases, we still notice that the particle loss remains distinctive among the simulated materials.

By using restrictive plane c, we further decrease the incident angle and we obtain the simulation results as written down in Table 5. In comparison with Table 4, restrictive plane c yields a non-significant change in terms of the characteristic parameters containing the particle loss, which also means that the variation rate of the characteristic parameters is expected to be insignificant beyond restrictive plane c.

Table 5. Point - plane scheme, restrictive plane c, thickness=10 cm.

Material	$\bar{\theta} \pm \delta\theta$ [mrad]	θ_{RMS} [mrad]	$\#_{\mathrm{Capture}}^{\mathrm{In-target}} \pm \delta$Capture	$\#_{\mathrm{Loss}}^{\mathrm{Off-target}} \pm \delta$Loss
Aluminum	16.1±27.4	31.7	-	35±6
Iron	36.0±50.6	62.1	1215±35	107±10
Copper	40.4±58.0	70.6	1216±35	193±14
Lead	64.5±86.0	107.5	1287±36	793±28
Uranium	79.7±96.1	124.8	3764±61	1059±33

It is noteworthy to mention that a partial transition from the particle loss to the particle absorption is perceptible according to Tables 3-5 especially if the VOI material is a potent absorber since the low-energy muons that lead to the particle loss in the wide beams typically have the absorption potential when interacting with the VOI material in the narrow beams, which also means that a certain portion o the particle loss is converted into the particle absorption in the VOI material towards restrictive plane c.

Table 6. Plane - plane scheme, restrictive plane a, thickness=10 cm.

Material	$\bar{\theta} \pm \delta\theta$ [mrad]	θ_{RMS} [mrad]	$\#_{\mathrm{Capture}}^{\mathrm{In-target}} \pm \delta$Capture	$\#_{\mathrm{Loss}}^{\mathrm{Off-target}} \pm \delta$Loss
Aluminum	15.2±26.0	30.1	-	1196±35
Iron	33.4±48.1	58.5	1092±33	1575±40
Copper	37.5±55.6	67.0	1118±33	1728±42
Lead	59.9±83.3	102.6	1206±35	2624±51
Uranium	74.0±92.8	118.7	3352±58	3299±57

In the next step, we continue with the plane - plane scheme, and Table 6 lists the simulation outcomes for restrictive plane a. In spite of the schematic change, we see that the characteristic parameters excluding the particle loss do not exhibit a significant difference. On the other hand, the particle loss via restrictive plane a within the plane - plane interplay results in the increased values as displayed in Table 6 in contrast to Tables 3-5.

Table 7. Plane - plane scheme, restrictive plane b, thickness=10 cm.

Material	$\bar{\theta} \pm \delta\theta$ [mrad]	θ_{RMS} [mrad]	$\#_{\mathrm{Capture}}^{\mathrm{In-target}} \pm \delta$Capture	$\#_{\mathrm{Loss}}^{\mathrm{Off-target}} \pm \delta$Loss
Aluminum	16.1±27.6	31.9	-	138±12
Iron	35.4±50.1	61.4	1206±35	430±21
Copper	39.9±57.9	70.3	1220±35	581±24
Lead	63.3±84.6	105.7	1327±36	1423±38
Uranium	78.4±94.6	122.9	3699±61	1926±44

So as to demonstrate the impact of the position change in the planar restriction for this scheme, the simulation results via restrictive plane b are tabulated in Table 7, and we experience a similar trend compared to the point-plane scheme that induces a drastic diminution in the particle loss along with the tiny variations in the rest of the characteristic parameters. As a means to complete our quantitative investigation for the plane - plane scheme, the simulation results for restrictive plane c are listed in Table 8, and we face a close trend as opposed to

Table 5, which also means that the reduction rate in the particle loss is decreased together with the very minor variations in the remaining characteristic parameters.

Table 8. Plane - plane scheme, restrictive plane c, thickness=10 cm.

Material	$\bar{\theta} \pm \delta\theta$ [mrad]	θ_{RMS} [mrad]	$\#^{\mathrm{In-target}}_{\mathrm{Capture}} \pm \delta$Capture	$\#^{\mathrm{Off-target}}_{\mathrm{Loss}} \pm \delta$Loss
Aluminum	16.3±27.4	31.8	-	88±9
Iron	36.1±50.8	62.3	1249±35	263±16
Copper	40.4±57.6	70.4	1258±35	389±20
Lead	64.5±86.1	107.6	1358±37	1164±34
Uranium	80.1±96.2	125.2	3833±62	1537±39

In the long run, our last simulations are devoted to investigate the thickness effect by solely using restrictive plane b since we aim at optimizing the particle loss with an ideal angular acceptance. Thus, Table 9 shows the characteristic parameters that are acquired by means of the point - plane scheme as well as restrictive plane b for a thickness of 40 cm with the same material group.

Table 9. Point - plane scheme, restrictive plane b, thickness=40 cm.

Material	$\bar{\theta} \pm \delta\theta$ [mrad]	θ_{RMS} [mrad]	$\#^{\mathrm{In-target}}_{\mathrm{Capture}} \pm \delta$Capture	$\#^{\mathrm{Off-target}}_{\mathrm{Loss}} \pm \delta$Loss
Aluminum	27.9±37.2	46.5	3046±55	93±10
Iron	58.2±67.9	89.4	10365±102	528±23
Copper	65.1±75.0	100.1	11072±105	588±24
Lead	102.6±112.0	152.6	11036±105	2210±47
Uranium	121.1±121.5	171.5	20371±143	3084±55

From Table 9, we numerically demonstrate that all the characteristic parameters increase as a function of thickness, and we find the most notable rise in the particle absorption. Finally, Table 10 lists the simulation results through the plane-plane scheme for the same thickness, and we see that the second scheme is not significantly different from the initial scheme with regard to the characteristic parameters omitting a higher number of the particle loss.

Table 10. Plane - plane scheme, restrictive plane b, thickness=40 cm.

Material	$\bar{\theta} \pm \delta\theta$ [mrad]	θ_{RMS} [mrad]	$\#^{\mathrm{In-target}}_{\mathrm{Capture}} \pm \delta$Capture	$\#^{\mathrm{Off-target}}_{\mathrm{Loss}} \pm \delta$Loss
Aluminum	28.0±37.6	46.9	3080±55	272±16
Iron	58.4±68.4	89.9	10599±103	1086±33
Copper	65.22±77.1	101.0	11341±106	1184±34
Lead	101.9±113.2	152.3	11341±106	3341±58
Uranium	120.1±121.9	171.1	20867±144	4181±65

6. Conclusion

All in all, we set out our restrictive generation scheme and we optimize the particle loss by keeping an angular acceptance that is directly dependent on the VOI geometry as well as the vertical position of the restrictive plane for a tomographic system of a finite size. Upon our simulation outcomes, we show that the particle generation by means of restrictive planes is an effective strategy that is flexible towards a variety of computational objectives in GEANT4. Into the bargain, we explicitly observe that the off-target loss is a characteristic parameter that varies in an ascending order from aluminum to uranium.

References

[1] Pesente S, Vanini S, Benettoni M, Bonomi G, Calvini P, Checchia P, Conti E, Gonella F, Nebbia G, Squarcia S *et al.* 2009 *Nuclear Instruments and Methods in Physics Research Section A: Accelerators, Spectrometers, Detectors and Associated Equipment* **604** 738–746
[2] Procureur S 2018 *Nucl. Instr. Meth. A* **878** 169
[3] Bonechi L, D'Alessandro R and Giammanco A 2020 *Reviews in Physics* **5** 100038
[4] Hagmann C, Lange D and Wright D Cosmic-ray shower generator (CRY) for Monte Carlo transport codes *2007 IEEE Nuclear Science Symposium Conference Record* vol 2 (IEEE) pp 1143–1146
[5] Heck D, Knapp J, Capdevielle J, Schatz G, Thouw T *et al.* 1998 *Report fzka* **6019**
[6] Biallass P and Hebbeker T 2009 *arXiv preprint arXiv:0907.5514*
[7] Cullen D E 1974 *Nuclear Science and Engineering* **55** 387–400
[8] Nakagawa M and Mori T 1984 MORSE-DD, A Monte Carlo code using multi-group double differential form cross sections Tech. Rep. JAERI-M 84-126 Japan Atomic Energy Research Inst.
[9] Rivard M 2001 *Applied Radiation and Isotopes* **55** 775–782
[10] Boman E, Tervo J and Vauhkonen M 2004 *Physics in Medicine & Biology* **50** 265
[11] Shultis J K and Faw R E 2011 An MCNP primer Tech. rep. Manhattan, Kansas State University
[12] Haino S, Sanuki T, Abe K, Anraku K, Asaoka Y, Fuke H, Imori M, Itasaki A, Maeno T, Makida Y *et al.* 2004 *Physics Letters B* **594** 35–46
[13] Goorley T, James M, Booth T, Brown F, Bull J, Cox L, Durkee J, Elson J, Fensin M, Forster R *et al.* 2012 *Nuclear technology* **180** 298–315
[14] Agostinelli S, Allison J, Amako K, Apostolakis J, Araujo H, Arce P, Asai M, Axen D, Banerjee S, Barrand G *et al.* 2003 *Nuclear instruments and methods in physics research section A: Accelerators, Spectrometers, Detectors and Associated Equipment* **506** 250–303
[15] Yáñez B O and Aguilar-Arevalo A A 2021 *Nucl. Instr. Meth. A* **987** 164870
[16] Forster R and Godfrey T 1985 MCNP - a general Monte Carlo code for neutron and photon transport *Monte Carlo Methods and Applications in Neutronics, Photonics and Statistical Physics* (Springer) pp 33–55
[17] Adam W, Bergauer T, Dragicevic M, Friedl M, Frühwirth R, Hänsel S, Hrubec J, Krammer M, Oberegger M, Pernicka M *et al.* 2009 *Journal of Instrumentation* **4** P06009
[18] Carlisle T, Cobb J and Neuffer D 2012 Multiple Scattering Measurements in the MICE Experiment Tech. Rep. FERMILAB-CONF-12-171-APC Fermi National Accelerator Lab. (FNAL), Batavia, IL (United States)
[19] Nugent J C 2017 *Multiple Coulomb scattering in the MICE experiment* Ph.D. thesis University of Glasgow
[20] Poulson D, Bacon J, Durham M, Guardincerri E, Morris C and Trellue H R 2019 *Philosophical Transactions of the Royal Society A* **377** 20180052
[21] Hohlmann M, Ford P, Gnanvo K, Helsby J, Pena D, Hoch R and Mitra D 2009 *IEEE Transactions on Nuclear Science* **56** 1356–1363